Leveraging microfluidic dielectrophoresis to distinguish compositional variations of lipopolysaccharide in *E. coli*

1 **Qianru Wang[1†,a], Hyungseok Kim[1†], Tiffany M. Halvorsen[2,b], and Cullen R. Buie[1*]**

2 [1]Department of Mechanical Engineering, Massachusetts Institute of Technology, Cambridge, MA,
3 USA.

4 [2]Department of Molecular, Cellular and Developmental Biology, University of California Santa
5 Barbara, Santa Barbara, CA, USA.

6 [†]These authors have contributed equally to this work and share first authorship.

7 ***Correspondence:**
8 Prof. Cullen R. Buie
9 crb@mit.edu

10 **Keywords: lipopolysaccharide, dielectrophoresis, linear electrokinetics, outer membrane**
11 **permeability, colistin susceptibility**

12 **Abstract**

13 Lipopolysaccharide (LPS) is the unique feature that composes the outer leaflet of the Gram-negative
14 bacterial cell envelope. Variations in LPS structures affect a number of physiological processes,
15 including outer membrane permeability, antimicrobial resistance, recognition by the host immune
16 system, biofilm formation, and interbacterial competition. Rapid characterization of LPS properties is
17 crucial for studying the relationship between these LPS structural changes and bacterial physiology.
18 However, current assessments of LPS structures require LPS extraction and purification followed by
19 cumbersome proteomic analysis. This paper demonstrates one of the first high-throughput and
20 noninvasive strategies to directly distinguish *Escherichia coli* with different LPS structures. Using a
21 combination of three-dimensional insulator-based dielectrophoresis (3DiDEP) and cell tracking in a
22 linear electrokinetics assay, we elucidate the effects of structural changes in *E. coli* LPS

---

[a] Present address: Department of Cardiovascular Medicine, Stanford University, Stanford, CA, USA.
[b] Present address: Lawrence Livermore National Laboratory, Livermore, CA, USA.

oligosaccharides on electrokinetic mobility and polarizability. We show that our platform is sufficiently sensitive to detect the LPS structural variations at molecular levels. To correlate the electrokinetic properties of LPS with the outer membrane permeability, we further examined the effects of LPS structural variations on bacterial susceptibility to colistin, an antibiotic known to disrupt the outer membrane by targeting LPS. Our results suggest that microfluidic electrokinetic platforms employing 3DiDEP can be a useful tool for isolating and selecting bacteria based on their LPS glycoforms. Future iterations of these platforms could be leveraged for rapid profiling of pathogens based on their surface LPS structural identity.

1 Introduction

Lipopolysaccharide[1] (LPS) is a glycolipid and the distinguishing feature of the outer membrane of Gram-negative bacteria, comprising over 75% of the cell surface in *E. coli* and *Salmonella*.[2,3] LPS forms the outer leaflet of the outer membrane and is an efficient permeability barrier to compounds such as antimicrobial peptides (AMPs). The chemical and structural diversity of LPS molecules is critical for the survival of pathogenic bacteria, which live similarly diverse lifestyles.[4] Indeed, many bacteria have evolved the ability to modify LPS in response to changes in environmental conditions, which leads to adaptive changes in outer membrane permeability, antibiotic resistance, and acts as a means to evade the human immune response.[2–5] Importantly, by studying LPS structural changes and their impact on the pathogenic lifestyle, new therapeutic treatments targeting LPS modifying enzymes have been proposed.[6]

LPS consists of three regions: lipid A, the core oligosaccharide, and a distal polysaccharide exhibiting the most inter-strain heterogeneity (termed O-antigen)[4] (Figure 1a). Lipid A is an amphipathic lipid consisting of a hexa-acylated glucosamine diphosphate headgroup that is *bis*-phosphorylated in *E. coli*. The phosphate substituents of lipid A mediate salt bridge formation with divalent cations (Ca^{2+} and Mg^{2+}), which are crucial to stabilize the outer membrane.[4,5] Attached to lipid A via a 3-deoxy-D-manno-oct-2-ulosonic acid (Kdo) linkage is the core oligosaccharide, which can be further divided into the inner and outer core regions. In *E. coli*, the inner core region contains Kdo and heptose.[4,7,8] Due to the presence of phosphate and carboxyl groups decorating these residues, the inner core is highly negatively charged. The outer core contains glucose and heptose,[7] and displays more variations in sugar composition and arrangement. Attached to the outer core is the more structurally diverse O-antigen, a long carbohydrate polymer built from a modal distribution of

53 repeating short oligosaccharide monomers.[4,9] O-antigen plays important roles in virulence and
54 resistance to AMPs.[9–11]

55 Genetically induced chemical modifications can occur within each region of the LPS molecule to
56 cope with environmental stressors, and are key to the survival and persistence of pathogens in human
57 hosts.[4] A more complete understanding of these adaptive cell envelope changes would aid in
58 therapeutic development, because LPS alterations affect small molecular uptake. For example,
59 phosphorylation and acylation of lipid A are capable of modulating outer membrane
60 permeability.[3,12,13] Moreover, addition of charged moieties or removal of sugars from the core
61 oligosaccharide drives resistance to cationic AMPs by disrupting electrostatically-driven membrane
62 association.[7,12,14] Finally, a large diversity of O-antigen modifications lead to inter- and intra-strain
63 LPS compositional variations, which is not only an indicator of virulence, but also arms the
64 pathogens by facilitating colonization and bypassing host defense mechanisms during infection.[3,9,10]

65 It is important to understand LPS structural versatility because its composition drives AMP resistance
66 and evasion of the host immune response.[5,9,12] However, a better understanding of LPS structural
67 adaptability is hindered by the lack of efficient LPS phenotyping approaches. Conventional methods
68 to characterize LPS, such as gel electrophoresis[15] and mass spectrometry[16], require prerequisite steps
69 for LPS extraction and purification from cell lysates, which is time-consuming, laborious, and
70 requires use of hazardous reagents and large sample volumes. Microfluidics is a powerful tool to
71 overcome this issue as it enables accurate and high-throughput manipulation of small sample
72 volumes. Previous attempts to characterize LPS with microfluidics have used platforms
73 functionalized with bio-recognition ligands, such as antibodies,[17] aptamers,[18] or AMPs,[19,20] which
74 bind specifically to LPS to enable pathotyping. In addition, microchip electrophoresis has been
75 applied to LPS structural analysis by facilitating LPS detection via fluorescent dye conjugation.[21,22]
76 However, reproducibility of these approaches relies on high-purity and repeatable LPS extraction and
77 separation. Although a variety of LPS extraction protocols have been developed[23], each method is
78 limited by size bias. For instance, the phenol–water extraction method[24] favors smooth LPS over
79 rough LPS, whereas the ether extraction method[25] favors the opposite. In addition, many of these
80 LPS extraction methods suffer from impurities, low yield, and contamination with proteins and
81 nucleic acids, which impede reliable application of the end product to sensitive downstream analysis,
82 such as molecular and immunological experiments. Moreover, these methods often involve LPS

83 staining steps, which are time-consuming, toxic, expensive, and likely to induce chemical
84 modifications of LPS (e.g. silver staining).[23]

85 Microfluidic dielectrophoresis (DEP)[26–29] systems using DC electric fields allow studies of cell
86 surface properties exclusively[29–32], and have demonstrated robust efficacy in separating bacteria
87 based on a variety of surface-related properties, including surface chemical modifications,[32] biofilm
88 formation capabilities,[30] and antibiotic resistance[29]. Our previous work has shown that three-
89 dimensional insulator-based DEP (3DiDEP)[26,30,31] provides sensitive and effective distinction of
90 bacteria with differential expression of *c*-type outer-membrane cytochromes, which are known to be
91 responsible for extracellular electron transfer across the cell envelope, in electrochemically active
92 microorganisms.[31] Our technique offers sub-strain level resolution at low applied voltages, which
93 diminishes confounding secondary flow effects, such as Joule heating and induced charge
94 electroosmosis[33]. In addition to DEP, linear electrokinetic behaviors of bacteria are also affected by
95 cell surface appendages. Duval and Ohshima proposed an electrokinetic theory of diffuse soft
96 particles, in which the charged cell surface components, such as LPS or outer membrane proteins,
97 form a soft polyelectrolyte layer around the cell.[34,35] Charge conditions and the spatial arrangement of
98 polyelectrolyte segments in the soft layer substantially affect cell electrokinetics, suggesting that
99 whole-cell electrokinetic mobility can be a biomarker to distinguish LPS structural variations. This
100 model has been applied to distinguish *E. coli* producing different fimbriae and pilus[36] and
101 *Acidithiobacillus ferrooxidans* grown with different metal ions[37].

102 In this work, we demonstrate the efficacy of 3DiDEP as a high-throughput and noninvasive approach
103 to probe bacterial LPS structural modifications. Using 3DiDEP and linear electrokinetics, we assayed
104 several *E. coli* K-12 strains deficient in synthesizing LPS core components, in addition to a parental
105 strain as a wild type reference and an O-antigen expressing strain. We show that compositional
106 variations in LPS structures drive changes in electrokinetic properties of the cell surface (i.e.
107 polarizability and linear electrokinetic mobility), resulting in a measurable metric for predicting cell
108 surface properties. With further investigations on colistin-mediated outer membrane
109 permeabilization, we observe a distinct correlation between the electrokinetic properties of *E. coli*
110 cells and their susceptibility to colistin, with colistin sensitivity increasing with cell polarizability.
111 We demonstrate that cell surface polarizability and electrokinetic mobility can be used as a proxy for
112 selecting bacteria based on their LPS structures in DEP-based systems, which will open a broader

113 avenue for downstream molecular and proteomic analysis to elucidate mechanisms underlying LPS
114 modifications and adaptive resistance to AMPs.

115 2 Materials and methods

116 2.1 LPS mutation and plasmid construction

117 *E. coli* K-12 LPS *waa* mutations were constructed in the Hayes lab at UCSB following the study by
118 Halvorsen et al.[38] Briefly, the *waaC* and *waaP* mutant strains were generated by Lambda Red-
119 mediated recombineering: a kanamycin-resistance cassette flanked by homology arms for the up- and
120 downstream regions of each gene was first cloned into an intermediate plasmid, then PCR amplified
121 to generate a linear fragment for recombination. To generate the *waaF* mutant strain, linear fragments
122 containing a kanamycin resistance gene with homology arms were PCR amplified from the
123 respective Keio collection deletion strains[39] and used as described above. To create an arabinose-
124 inducible *waaC* complemented strain, the *waaC* mutant was transformed with plasmid pCH450-
125 P_{BAD}*waaC* or an empty plasmid (pCH450). Expression of these plasmids are suppressed in the
126 presence of glucose. Because the addition of arabinose caused a growth defect in the *waaC*
127 complemented strain but removing glucose was sufficient to complement the *waaC* deletion, we
128 chose to use the latter to complement.

129 2.2 Bacterial strains

130 Bacterial strains and plasmids used in this study are listed in Supplementary Table 1. Following the
131 study by Halvorsen et al.[38], all bacterial cells were inoculated from frozen stocks, and single colonies
132 were grown in LB at 37°C overnight, back-diluted 1:100 and grown to mid-log phase before
133 harvesting for 3DiDEP analysis. Where appropriate, media were supplemented with antibiotics at the
134 following concentrations: kanamycin (Kan), 50 µg/mL (Sigma-Aldrich); streptomycin (Str), 50
135 µg/mL (Sigma-Aldrich); spectinomycin (Spm), 100 µg/mL (Sigma-Aldrich); and tetracycline (Tet),
136 15 µg/mL (Sigma-Aldrich). To achieve a dynamic control of *waaC* expression in the *waaC*-
137 complementary strain (Δ*waaC* + *pwaaC*), both strain Δ*waaC* + EV (control for plasmid burden) and
138 strain Δ*waaC* + *pwaaC* were grown with 0.4% glucose overnight, pelleted at 4000 rpm for 4 minutes,
139 washed twice with plain LB, and resuspended separately in LB with and without glucose with an
140 initial OD_{600} of 0.1.

141 2.3 Sample preparation

142 Cells grown to mid-log phase were fluorescently labeled using 20 μM SYTO™ BC Green
143 Fluorescent Nucleic Acid Stain (Thermo Fisher Scientific) in their growth medium, incubated at
144 room temperature for at least 30 min without light exposure, and then centrifuged at 4000 rpm for 4
145 min. The cells were rinsed once and well mixed using a vortex mixer to remove excessive dye before
146 being resuspended in the DEP buffer. The DEP buffer solution (final pH = 6.8) was prepared by
147 adding DI water to 1× phosphate-buffered saline until the solution conductivity was nearly 100
148 μS/cm. The DEP buffer also contains from 1 to 2% (v/v) glycerol to match the growth medium
149 osmolarity.

150 **2.4 Microchannel fabrication and preparation for electrokinetics**

151 Microfluidic devices for electrokinetic mobility measurements and 3DiDEP analysis were fabricated
152 in laser-cut poly(methyl methacylate) (PMMA) chips using a CNC controlled micro-mill
153 (Microlution), and bonded using a solvent-assisted bonding process[31] after cleaning with acetone,
154 methanol, isopropanol and deionized (DI) water in sequence. Both channel ends of the device were
155 then bonded with electrical-insulating sleeve washers (McMaster-Carr) using a 5-minute two-part
156 epoxy glue (Gorilla Glue). The sleeve washers serve as fluid reservoirs with a volume ~70 μL to
157 contain bacterial samples. After bonding, each microchannel was connected to a syringe using Tygon
158 tubing (McMaster-Carr) to flush and stabilize channel wall ("priming") with the following reagents
159 and conditions: 0.1 M potassium hydroxide, 1 mL/min, 10 mL; DI water, 1 mL/min, 10 mL; DEP
160 buffer, 800 μL/min, 7 mL.

161 **2.5 3DiDEP assay and image analysis**

162 3DiDEP trapping and derivation of trapping voltages have been described in our previous
163 studies[26,30,31]. Cells were resuspended in the DEP buffer at an OD_{600} of ca. 0.05 and quickly added
164 into the 3DiDEP microchannel via the fluidic reservoirs. A "linear sweep" DC voltage difference
165 increasing linearly with time at 1 V/s from 5 to 100 V was applied across the channel via an HVS-
166 448 high-voltage power supply (LabSmith), controlled by a customized LabVIEW program. The
167 SYTO BC fluorescence intensity increases with time as bacterial cells accumulate near the
168 constricted region (Supplementary Video 1) and was recorded by time-lapse image sequences
169 captured at 1 frame/s using a charge-coupled device (CCD) camera (CoolSNAP HQ2, Photometrics)
170 fitted to an inverted fluorescence microscope (Eclipse Ti-U, Nikon). The fluorescent intensity data
171 (background subtracted) near the constriction versus time (i.e., the applied voltage) were fit into a

172 polyline with two segments, whose intersection point was taken as a variable optimized using the
173 least squares method by a customized MATLAB R2015b (MathWorks) code. The applied voltage
174 corresponding to the best-fit intersection point was extracted as the trapping voltage (Figure 2) during
175 3DiDEP.

176 **2.6 Linear electrokinetic mobility**

177 To track the location of single cells and measure their linear electrokinetic mobility, a 500 μm × 60
178 μm × 1 cm (width × depth × length) straight microfluidic channel was designed and fabricated as
179 described above. Prepared bacterial samples were loaded into the fluid reservoirs of a primed
180 microchannel and fine-tuned until cell motion induced by gravity or pressure-driven flow was
181 minimized. A pair of platinum electrodes (LabSmith) was connected to each reservoir of the channel
182 to apply a constant DC voltage ranging from 10 to 50 V (with a 10 V increment) across the
183 microchannel using an HVS-448 high-voltage power supply (LabSmith). During the linear
184 electrokinetics, image sequences capturing cell movement in the microchannel was obtained using an
185 inverted microscope (Eclipse Ti-U, Nikon) equipped with a sCMOS camera (Andor, Oxford
186 Instruments) and image acquisition software (NIS-Element, Nikon). To minimize Joule heating
187 effects, the DC voltage was applied for less than one minute. To automatically extract cell locations
188 and velocities in the obtained image sequences, a particle tracking algorithm was implemented using
189 the python package trackpy[40] (Supplementary Figure 1a). First, image sequences were loaded using a
190 python package PIMS. Next, features of fluorescent single cells were identified and linked across the
191 entire time frame, creating trace information for each detected cell[41]. Cell traces either appearing in
192 less than five sequential frames or showing no increments in cell position with time were considered
193 as noise traces and removed. K-means clustering was applied in noise filtering to exclude cells stuck
194 to the channel wall. In order to derive linear electrokinetic mobilities and exclude background flow
195 noise, we used a 3D fitting model to decouple nonlinear effects induced by pressure-driven or
196 electrothermal flows. Data of single cell velocities, cell locations, and corresponding applied electric
197 fields were interpreted based on a physical model with an equation,

198 $$v(E,x) = \mu_{EK}E + cE(x^2 - Hx), \quad (1)$$

199 where v is the velocity, E is the magnitude of electric field, x is the distance of the cell measured
200 from the bottom channel wall, μ_{EK} is the electrokinetic mobility, H is the width of the microchannel,
201 and c is a constant (Supplementary Figure 1a and 1b). The quadratic term in the model equation

202 represents a parabolic-shaped flow profile depending on the cell location x, as an effort to decouple
203 the background nonlinear flow effects[33]. Using Equation 1, the best-fit parameter μ_{EK} was computed
204 as the linear electrokinetic mobility for each strain.

205 **2.7 Cell segmentation and polarizability**

206 Cell cultures grown to mid-log phase were centrifuged at 4000 rpm for 4 minutes, and concentrated
207 to reach an OD_{600} of ~ 3. SYTO™ BC Green Fluorescent Nucleic Acid Stain (Thermo Fisher
208 Scientific) was added to the cell samples with a final concentration of 0.1% v/v, and cells were
209 stained in the dark at room temperature for 30 min. To immobilize the cells during imaging, 2 μL of
210 the cell suspension was placed at the center of a 24 × 50 mm^2 coverslip and covered by a thin 1%
211 agarose pad (1 × 10 × 10 mm^3)[42]. Images were taken using the inverted microscope (Eclipse Ti-U,
212 Nikon) with a 100X or 150X objective.

213 With the obtained images, cell segmentation was performed using Coli-Inspector[43], an add-on project
214 to an image analysis software (ImageJ) and its plugin (ObjectJ). At least 400 single cells were
215 identified to measure their length and diameter (i.e. long and short axis). The measurements were
216 used to calculate the Perrin friction factor (ζ) and cell shape factor[31] (Figure 3c, Supplementary
217 Information). Average cell shape factor and DEP mobility for each strain were used to derive the
218 Clausius-Mossotti factor, a measure of the cell polarizability (Figure 3b, Supplementary Figure 2).

219 **2.8 Colistin susceptibility and growth**

220 *E. coli* strains varying in LPS composition were investigated for susceptibility to colistin. Each strain
221 was grown overnight (see section "Bacterial strains" in Methods) and diluted to OD_{600} ~0.1. To
222 prepare a minimum inhibitory concentration (MIC) assay, colistin was added to 150 μL LB
223 containing streptomycin (replaced by spectinomycin for the O-antigen expressing strain) per strain to
224 reach a final concentration ranging from 0.0156 to 2 μg/mL (with a two-fold increment) in a clear
225 flat-bottom 96-well plate (Corning). Then, aliquots of 1.5 μL bacterial samples were added to the
226 multiwell plate and covered with a sealing film (Breathe-Easy). Cell abundance in the multiwell was
227 measured every 10 minutes by optical density at 600 nm using a microplate spectrophotometer
228 (Epoch 2, Biotek). Each microplate was incubated at 37°C for 20 hours in shaking mode. Three
229 biological samples were repeated for each strain and colistin concentration. Based on the bacterial
230 abundance at the final time measurement, MIC of colistin was determined by strain turbidity, and cell
231 growth was analyzed by a function of x μg/mL colistin concentration with the following equation,

232 $$\text{Growth ratio (\%)} = \frac{\text{Final cell abundance at colistin } x \text{ μg/mL}}{\text{Final cell abundance without colistin}} \times 100\%. \quad (2)$$

233 A maximal growth rate was calculated based on the time-series abundance. First, local growth rates
234 were computed as the time derivatives of the natural logs of cell OD_{600} using data points collected
235 every three timepoints. Then the maximum local growth rate calculated within the entire 20-hour
236 time window was obtained for each studied strain.

237 **2.9 Outer membrane permeability assay**

238 A 1-N-phenylnaphthylamine (NPN) uptake assay was performed to compare the effects of
239 differential LPS structures on colistin-mediated permeabilization of outer membranes in the studied
240 strains using a protocol adapted from MacNair et al.[44] In brief, bacterial cells in mid-log phase were
241 washed twice with 5 mM HEPES buffer (pH ~7.2, Sigma-Aldrich) containing 20 mM glucose and
242 adjusted to have their OD_{600} reach about 0.4. One hundred microliters of cells were added to 100 μL
243 HEPES buffer containing 20 μM NPN and a varying concentration of colistin (ranging from 0.39 to
244 200 μg/mL, two-fold of the final concentrations) in a black clear flat-bottomed 96-well plate. After
245 allowing the microplate to sit for an hour at room temperature without light exposure, NPN
246 fluorescence levels were read using a Varioskan Flash plate reader (Thermo Scientific) with an
247 excitation and emission wavelengths of 355 ± 5 nm and 420 ± 5 nm, respectively. Three biological
248 replicates were repeated for each strain and colistin concentration. The NPN uptake factor was
249 calculated as the ratio of background-subtracted fluorescence (subtracted by the fluorescence levels
250 in the absence of NPN) values of the bacterial suspension and of the suspending medium.[45] Then, the
251 NPN uptake factor was normalized by a cell abundance factor to exclude the fluorescence increase
252 induced by cell growth. The cell abundance factor was estimated using the maximal growth rate
253 derived from the colistin susceptibility assay as described above (see section "Colistin susceptibility
254 and growth" in Methods). The cell abundance factor is larger than 1 for cases exhibiting a positive
255 growth rate where colistin concentration was lower than the MIC. Finally, fractional changes of
256 normalized NPN uptake (Figure 5) for the O-antigen expressing strain and each core mutant strain
257 relative to the parental strain were calculated as

258 $$\text{Relative difference in NPN uptake (\%)} = \frac{\text{NPN uptake of mutant - NPN uptake of parental strain}}{\text{NPN uptake of parental strain}} \times 100\% \quad (3)$$

259 to analyze the effects of LPS structural variations on outer membrane permeability to colistin.

260 **3 Results and Discussion**

261 **3.1 LPS compositional variations drive changes in *E. coli* electrokinetic properties**

262 Due to the presence of LPS and other external appendages, bacteria moving in electrolyte solutions
263 act as so-called soft particles, i.e. hard particles covered by an ion-permeable polyelectrolyte layer
264 (PEL),[34,46] in which both the distribution of charge density and the arrangement of LPS monomers
265 can substantially affect cell electrokinetic properties.[35] Not only the spatial details of phosphate
266 groups in Lipid A and LPS inner core but also electroneutral sugar residues in the outer core and O-
267 antigen (Figure 1a) confer an inhomogeneous distribution of polyelectrolyte segments within the
268 PEL. According to the electrokinetic theory of diffuse soft particles by Duval and Ohshima,[34,35]
269 electrophoretic mobility of a soft particle increases with an increasing volumetric charge density
270 (ρ_{PEL}) or a decreasing δ, where δ represents the degree of inhomogeneity measured by the width of
271 distribution of uncharged segments near the front edge of the PEL. In addition, PEL segments can be
272 considered as resistance centers exerting Stoke's drags on the liquid flowing within the PEL with a
273 frictional coefficient $\gamma \sim \eta/(1/\lambda)^2$, η being the viscosity of the electrolyte solution.[34,35,46] The
274 electrophoretic softness, 1/λ, is a characteristic penetration length representing how easily the fluid
275 can flow through the PEL. Especially for the low electrolyte concentration used in this study,
276 electrokinetic behaviors of PEL become increasingly sensitive to the spatial distribution of the
277 polyelectrolyte segments.[34]

278 We hypothesize that LPS structural differences in bacteria can be manifested in their PEL volumetric
279 charge density (ρ_{PEL}), inhomogeneous distribution of polymer segments (δ), and electrophoretic
280 softness (1/λ), thereby leading to distinguishable electrokinetic behaviors. To test the hypothesis, we
281 studied several *E. coli* K-12 strains carrying differential LPS structures. In addition to a wild type
282 control (Parental strain in Figure 1), a K-12 strain with restored O-antigen synthesis[38,47] was selected
283 to model PEL with decreased charge density and enhanced polymer segment inhomogeneity. This
284 strain was established by transforming *E. coli* W3110 with pMF19, which carries the *wbbL* gene and
285 restores expression of O16 polysaccharide.[47] In addition, three "deep-rough" LPS mutants (Δ*waaC*,
286 Δ*waaF*, and Δ*waaP*)[38] were chosen to model scenarios with reduced PEL thickness and altered
287 charge conditions, as they are unable to synthesize the full LPS core (Figure 1a). WaaC[48] is the
288 heptose I transferase that acts prior to WaaF and WaaP during core biosynthesis. Deletion of *waaC*
289 results in a loss of the majority of the LPS core including the inner core phosphates. WaaF transfers a
290 heptose II to the inner core,[48] and its deletion causes a severely truncated LPS core but keeps the
291 heptose I phosphates in the inner core. WaaP is a kinase that phosphorylates heptose I and is also

292 required for subsequent phosphorylation of Heptose II and addition of Heptose III to the inner core.[1,8]
293 Loss of *waaP* removes Heptose III and strips all the phosphate groups off the inner core.

294 In order to detect these LPS structural variations by measuring whole-cell electrokinetic mobility, we
295 developed a particle tracking algorithm (see Methods) to extract the dependence of cell migration on
296 the applied electric field. The algorithm captures velocity, position within the microchannel, and the
297 corresponding applied voltages for each individual cell, and fits them using a 3D regression model to
298 decouple the confounding effects of pressure-driven flow and nonlinear electrokinetic flow
299 (Supplementary Figure 1a and 1b). Cell motion in the straight microchannel is driven by both the
300 background electroosmotic flow and electrophoresis of the cell. However, the background
301 electroosmotic flow is constant given the same counterion concentration and applied electric field at
302 the microchannel/medium interface,[49] leaving the linear electrokinetic mobility purely a function of
303 cell electrophoresis.

304 As shown in Figure 1b, the linear electrokinetic mobility of all the tested strains is negative, which
305 agrees with the electric properties of the charged groups (e.g. carboxyl and phosphate groups) in the
306 cell outer membrane and the LPS structures.[50,51] O-antigen restoration results in a significantly less
307 negative ($p = 0.00024$) electrokinetic mobility compared to the control strain lacking O-antigen. This
308 observation is consistent with our hypothesis that the longer electroneutral oligosaccharide on this
309 strain may decrease electrokinetic mobility by not only increasing the PEL thickness, thereby
310 lowering the volume charge density, but also by enhancing inhomogeneity of the polyelectrolyte
311 segment distribution in the PEL.

312 In contrast, the truncated LPS core present in the Δ*waaF* and Δ*waaP* mutants enhances cell
313 electrokinetic mobility relative to the parental strain by 48.7% ($p = 0.0023$) and 22.7% ($p = 0.012$),
314 respectively (Figure 1b). This is consistent with the increased electrophoretic mobility of bacteria due
315 to LPS removal after an EDTA treatment observed previously.[37] These results indicate that truncation
316 of LPS core components can lead to an increased PEL charge density, and thus a higher
317 electrokinetic mobility to a differential extent. For instance, the Δ*waaF* mutant carries additional
318 phosphate groups with shorter LPS length compared to Δ*waaP*, which is predicted to cause a stronger
319 elevation of charge density and a lower inhomogeneity of polyelectrolyte segment distribution in the
320 PEL relative to the control strain. Correspondingly, the Δ*waaF* mutant exhibits the strongest
321 electrokinetic mobility among tested strains (Figure 1b). In contrast, a *waaP*-deficiency is predicted

322 to cause a lower extent of increase in charge density relative to the control due to the loss of both
323 phosphates and Heptose III residues.

324 Compared to mutants Δ*waaF* and Δ*waaP*, deletion of *waaC* causes a more drastic LPS truncation
325 (Figure 1a), and correspondingly shows a significant decrease in electrokinetic mobility relative to
326 the other two mutants (p = 0.007 and 0.003, respectively). Interestingly, despite truncating the largest
327 LPS core in our mutant screen, the Δ*waaC* mutant exhibits an electrokinetic mobility comparable to
328 that of the parental strain with an intact core (p = 0.45). We hypothesize that a *waaC*-deficiency
329 generates an increased charge density but a decreased electrophoretic softness (1/λ), resulting in
330 stronger frictional forces exerted on the liquid flowing within the PEL, which could be compensatory
331 to each other in terms of their effects on the electrokinetic mobility. Comparable electrophoretic
332 mobilities have been reported previously between *E. coli* constitutively producing the long (10~100
333 μm) type-F pili and Ag43 proteins,[36] suggesting that cell electrokinetic mobility is affected both by
334 the length of cell surface appendages and the interplay between electrophoretic softness and spatial
335 arrangement of charged groups of the PEL. In deep-rough LPS mutants, physiological alterations
336 may also contribute to strain-specific signatures that are differentiable by 3DiDEP. For instance,
337 Δ*waaC* and Δ*waaF* mutations have been reported to cause a lower abundance of OmpC porin in the
338 outer membrane, whereas the *waaP* mutant expresses wild-type levels of OmpC.[38,52] OmpC
339 leverages negatively charged residues in its extracellular loops to induce cation selectivity.[53] The
340 lower abundance of OmpC in Δ*waaC* and Δ*waaF* cell outer membrane may have partially
341 compensated for the effect of LPS core truncation on charge density of surface soft layers, thereby
342 lowering their baseline values of electrokinetic mobility. It also reveals that characterizing LPS
343 properties on whole cells is beneficial for capturing physiological changes that are difficult to
344 observe when studying LPS alteration using purified LPS alone.

345 **3.2 Trapping *E. coli* based on LPS structures using 3DiDEP**

346 In addition to studying cell electrokinetic mobility, a property induced by cell surface charge, we next
347 investigated cell polarizability, which is the tendency of electric dipoles to form at the cell surface
348 (not necessarily charged) when subjected to externally applied electric fields. Cell polarizability has
349 been correlated with the extracellular electron transfer capability in electrochemically active bacteria
350 in our previous study[31], and has been proven to be a sensitive label-free biomarker to detect
351 variations in cell outer membrane components[30].

352 To measure cell polarizability, we used a microfluidic 3DiDEP trapping technique, incorporating
353 linear sweep analysis, in which the applied electric field increases linearly with time across the
354 microchannel (Figure 2a). The microchannel features a 3D hourglass shaped constriction at the
355 middle, which bridges two main channels. The 3D constriction has a cross-sectional area 100 times
356 smaller than that of the main channel, which creates a strong electric field gradient to enable a high
357 DEP force for immobilizing bacteria near the constriction[27,29,32,54,55]. In response to the linear sweep
358 voltage, bacteria flowing down the main channel start to slow down and gradually accumulate near
359 the constriction when DEP balances cell motion due to linear electrokinetics along the electric field
360 direction (Supplementary Video 1). The threshold voltage for the onset of cell immobilization,
361 termed the 'trapping voltage', is a measure of the comparison between cell DEP mobility and the
362 counteracting linear electrokinetic mobility. The criterion for 3DiDEP immobilization of a single cell
363 can be expressed as[26,28,29,31,55]

364 $$\mu_{EK}\vec{E}\cdot\vec{E}+\mu_{DEP}\left(\nabla\vec{E}^2\right)\cdot\vec{E}=0 \quad (4)$$

365 where μ_{EK} is the linear electrokinetic mobility, $\vec{E}$ is the local electric field corresponding to the
366 measured 3DiDEP trapping voltage, and μ_{DEP} is the DEP mobility. The studied *E. coli* K-12 strains
367 are rod shaped and can be modeled as ellipsoidal particles with semi-axes $a > b = c$[56] (Supplementary
368 Figure 2). Thus, the DEP mobility μ_{DEP} can be expressed as

369 $$\mu_{DEP}=\frac{b^2\varepsilon_m\kappa_{CM}}{3\eta\xi} \quad (5)$$

370 where ε_m and η are the permittivity and viscosity of the surrounding medium, respectively, and ξ is
371 the Perrin friction factor (see Supporting information for a detailed derivation). The Clausius-
372 Mossotti factor, κ_{CM}, is a measure of the relative polarizability of the cell compared to the
373 surrounding medium, and can be estimated from the experimentally determined 'trapping voltage'
374 required for initiating 3DiDEP cell trapping.

375 Our 3DiDEP measurement reports an inverse relationship between the length of *E. coli* K-12 LPS
376 and the trapping voltage for 3DiDEP cell immobilization (Figure 2b). The O-antigen expressing
377 strain requires a 55% lower trapping voltage relative to the parental strain ($p = 0.025$), and
378 correspondingly this strain expresses longer LPS with distal O-antigen repeats. In addition to the
379 lower electrokinetic mobility resulting from the O-antigen expression (Figure 1b), this can be
380 explained by a higher polarizability thereby a lower trapping voltage required to counteract with

381 linear electrokinetics, which will be shown in the following section. In contrast, the *waaC* mutant
382 strain requires the highest trapping voltage for 3DiDEP immobilization ($p = 0.025$, Figure 2b). To
383 confirm this relationship, we then measured trapping voltages of a *waaC* mutant strain complemented
384 with an empty vector (Δ*waaC* + EV) and a *waaC* mutant strain complemented with pCH450-*waaC*
385 grown with (Δ*waaC* + *pwaaC*, Glc+) or without glucose (Δ*waaC* + *pwaaC*, Glc-). Removal of
386 glucose in the growth medium complements *waaC* expression by de-repression of P_{BAD}, which is
387 expected to result in high levels of *waaC* expression and restore wild type levels of core synthesis
388 (Figure 1a). As expected, when grown with glucose (Glc+ in Figure 2b), the Δ*waaC* + *pwaaC* strain
389 shows a comparable trapping voltage ($p = 0.077$) relative to the isogenic control (Δ*waaC* + EV).
390 Removal of glucose (Glc-) in the growth medium restores the full-length LPS core, which results in a
391 65.7% drop in the trapping voltage ($p < 0.05$), further indicating that cells lacking *waaC* require a
392 stronger trapping voltage for 3DiDEP immobilization. The Δ*waaC* + EV strain ($p = 0.18$) and the
393 Δ*waaC* + *pwaaC* strain grown with glucose ($p = 0.65$) show comparable trapping voltage relative to
394 the parental strain, suggesting that the introduction of the vector pCH450 does not significantly affect
395 the cell polarizability. Furthermore, deletion of *waaF* and *waaP* lead to a 24.3% increase ($p = 0.025$)
396 and a 10.5% decrease ($p = 0.053$) in trapping voltage relative to the parental strain, respectively.
397 Although the consequence of *waaF* deletion should result in only one less phosphorylated heptose
398 when compared to a mutant lacking *waaC*, the Δ*waaF* mutant leads to a trapping voltage ~20% lower
399 than that of the Δ*waaC* mutant. Comparison between the trapping voltages of Δ*waaC* and Δ*waaF*
400 strains suggests that 3DiDEP trapping is sensitive enough to detect a single heptosylation event.
401 These data indicate that 3DiDEP can be used to selectively immobilize bacteria based on their LPS
402 length.

403 **3.3 LPS structural variations affect cell DEP mobility and polarizability**

404 To determine the cell polarizability, for each trapping voltage measurement, we performed additional
405 particle image velocimetry (PIV) analysis[31] for cell motion in the corresponding main channel region
406 (where the electric field is uniform). Electrokinetic mobilities measured by this PIV analysis show a
407 high consistency with the results measured using our cell tracking algorithm (Supplementary Figure
408 1c). Incorporating the electrokinetic mobility and the corresponding threshold electric field
409 numerically computed from the measured trapping voltages (Equation 4), we derived the DEP
410 mobilities for all the tested strains (Figure 3a and Supplementary Figure 3). To decouple the effects
411 of cell size/shape, we computed the Clausius-Mossotti factor (κ_{CM}) as a measure of cell polarizability

412 (Equation 5, Supplementary Figure 2) using cell shape parameters (b and ξ) measured for all the
413 tested strains using high magnification microscope images (see Methods).

414 Our results show that the O-antigen expressing strain possesses a higher DEP mobility (by 66.8%, p
415 = 0.025, Figure 3a and Supplementary Figure 3) and a higher κ_{CM} (by 98.1%, p = 0.00024, Figure
416 3b) but a lower electrokinetic mobility (by 27.8%, p = 0.00024) relative to the parental strain (Figure
417 2b), suggesting that the presence of O-antigen not only lowers the negative charge density but also
418 enhances the polarizability of the cell surface. In contrast, although knocking out *waaC* does not
419 significantly affect cell electrokinetic mobility (Figure 1b), its removal decreases the DEP mobility
420 by 34.2% (p = 0.025) and polarizability by 16.4% (p = 0.015). As discussed above, the presence of
421 LPS adds a charged soft PEL layer around a bacterium. Ion transport in this soft PEL layer and
422 electrical double layer jointly contribute to the induced dipole moment coefficient. As demonstrated
423 in our previous study,[57] fibrillated strains with a thicker PEL have a higher induced dipole moment
424 coefficient and thereby are more polarizable than unfibrillated strains in the low electrolyte
425 concentration regime, which agrees with our observation that long LPS chains resulting from O-
426 antigen expression leads to a higher polarizability but truncating most of the LPS core via *waaC*
427 deletion results in a significantly lower polarizability (Figure 3a and 3b). Interestingly, deletion of
428 *waaP* increases all three parameters that we tested, showing an enhanced DEP mobility (by 41.6%, p
429 = 0.025), polarizability (by 57.6%, p = 0.00076), and electrokinetic mobility (by 22.7%, p = 0.012).
430 By comparison, the mutant strain lacking *waaF* exhibits the strongest increase in cell electrokinetic
431 mobility (p = 0.0023) among all of the examined LPS mutations, a 47.3% increase in polarizability (p
432 = 0.0013), but small changes in DEP mobility (p = 0.18). These results indicate that not only the PEL
433 thickness but also the polyelectrolyte segment distribution drive changes in cell polarizability. The
434 polar to nonpolar composition of the LPS chains affects the conductivity distribution in the PEL,
435 thereby influencing cell polarizability, which is consistent with the discrepancies observed between
436 parental strain and mutants lacking *waaF* and *waaP* (Figure 3b). It is interesting to note that the three
437 core mutants exhibit altered morphology relative to the parental strain (Figure 3c). Because cell shape
438 can affect both the drag force via the Perrin friction factor (ζ)[58] and the DEP force via the short semi-
439 axis (b) of the cell, the ratio ξ/b^2 (Figure 3c) represents how much the ellipsoidal cell shape
440 influences the drag force versus the DEP force.[31] Note that deletion of *waaF* does not affect DEP
441 mobility significantly but drastically increases polarizability, indicating that the enhanced
442 polarizability can also be attributed to the morphological change induced by this mutant.

443 **3.4 Outer membrane permeability increases with cell polarizability**

444 After characterizing the differential electric and dielectric properties of *E. coli* strains conferred by
445 their LPS structural variations, we next sought to examine whether changes in polarizability and
446 electrokinetic mobility are associated with variations of outer membrane permeability against
447 membrane-disrupting reagents, such as antibiotics. We hypothesize that cells capped with thick PEL
448 layers with small electrophoretic softness, i.e. less penetrable by liquid flow, carry less permeable
449 outer membranes, and thereby are distinguishable by an increased cell polarizability and altered
450 electrokinetic properties. To test this hypothesis, colistin was chosen as the antibiotic agent, as it is
451 known to interact with the bacterial outer membrane by destabilizing LPS.[59] The activity of colistin
452 starts with electrostatic interaction between the positive charges carried by colistin and the negatively
453 charged phosphates in LPS, which is believed to displace divalent cations (Ca^{2+} and Mg^{2+}) that are
454 important to bridge and stabilize the LPS layer.[60]

455 To determine cell susceptibility to colistin, we measured minimum inhibitory concentrations (MIC)
456 and cell growth (cell abundance normalized by values when colistin is absent) across a varying
457 colistin level for each strain (Figure 4). As expected, *E. coli* expressing O-antigen shows the highest
458 MIC (Figure 4a) and the highest growth ratio at all colistin levels (Figure 4b) among the tested
459 strains. The parental strain shows an MIC of 0.33 μg/mL and a cell abundance decreased by 80%
460 when the colistin concentration reaches 0.25 μg/mL, whereas the O-antigen expressing strain shows a
461 two-fold increase in MIC compared to the parental strain, and keeps a high abundance (99%) at 0.25
462 μg/mL colistin. The enhanced resistance to colistin suggests that the presence of O-antigen facilitates
463 the barrier function of the outer membrane against colistin, which is consistent with the high
464 polarizability and low electrokinetic mobility observed for this strain. Electrostatic interactions
465 between the cationic groups in colistin and phosphate groups in Lipid A play important roles in
466 peptide binding.[44] The presence of O-antigen decreases cell electrokinetic mobility (Figure 1b) and
467 increases polarizability (Figure 3b), which indicates a lower charge density and/or a higher friction
468 factor in the soft PEL layer, and thereby may have shielded the electrostatic effects and impeded
469 colistin activity. In contrast, mutants lacking genes *waaC*, *waaF* or *waaP* exhibited a significantly
470 lower growth in response to colistin compared to the parental strain (p = 4.0E-7, 3.8E-7, and 0.0006
471 respectively, two-way ANOVA), which can be explained by the absence of outer core
472 oligosaccharides. Among these deep-rough LPS mutants, the Δ*waaC* strain shows the lowest MIC
473 followed by the Δ*waaF* and Δ*waaP* strains (Figure 4a, p = 0.0005). A similar trend was found in
474 colistin-mediated cell lysis of the Δ*waaC*, Δ*waaF* and Δ*waaP* strains (Figure 4b) as well as in their

475 DEP mobilities and polarizabilities (Figure 3a and 3b). These results suggest a correlation between
476 cell susceptibility to colistin and LPS composition, which is distinguishable by their polarizability
477 and electrokinetic properties.

478 To further investigate the correlation between cell electrokinetic properties and outer membrane
479 permeability, we measured the uptake of 1-N-phenylnaphthylamine (NPN), a nonpolar probe that
480 fluoresces under a phospholipid condition inside of the outer membrane,[45] for each strain in the
481 presence of colistin (Figure 5). An intact outer membrane prevents NPN from entering the
482 phospholipid layer and the subsequent fluorescence.[44] To examine if cells that differ in polarizability
483 and electrokinetic mobility can be distinguished by their differential outer membrane permeability,
484 we treated the *E. coli* strains with NPN and various concentrations of colistin, and measured the
485 fluorescence after one hour of incubation. To decouple the possible effects of increased cell
486 abundance (due to low colistin concentrations, Figure 4b) on NPN fluorescing, NPN uptake values
487 were normalized by a cell abundance factor estimated from the maximal growth rate (Supplementary
488 Figure 4, see Methods).

489 Figure 5a and 5b show the relative differences of NPN uptake calculated for each tested strain
490 compared to the parental strain. As expected, the O-antigen expressing strain shows a strong decrease
491 in its NPN uptake, by a factor of 15.7% to 53.3% compared to the parental strain, across all colistin
492 concentrations (Figure 5a), indicating that the presence of O-antigen prevents NPN from entering the
493 outer membrane. Conversely, mutants harboring truncated LPS show an increased NPN uptake even
494 in the absence of colistin, indicating a compromised outer membrane with enhanced permeability to
495 NPN. In addition, it has been reported that mutants expressing severely truncated LPS cores fail to
496 insert many outer membrane proteins and consequently have to fill the "void" in the outer membrane
497 with phospholipids,[61] which also explains why their NPN fluorescence is stronger than the control
498 even without colistin exposure (Figure 5b). Moreover, we observed a lower tolerance for colistin-
499 mediated membrane disruption in the *waa* mutants compared to the parental strain, and the
500 membrane disruption dynamics vary at different colistin levels. For instance, at a colistin
501 concentration of 0.195 μg/mL, a stronger increase of NPN uptake was observed by ~two-fold for
502 Δ*waaC* and Δ*waaF*, and 67.5% for Δ*waaP*, respectively. The enhancement of NPN uptake caused by
503 these mutants gradually decreases when colistin concentration increases up to 1 μg/mL (Figure 5b).
504 This agrees with the distinct colistin susceptibility between the parental and mutant strains shown in
505 Figure 4b. For example, cells are completely depleted at 0.031, 0.063, and 0.125 μg/mL colistin for

506 Δ*waaC*, Δ*waaF*, and Δ*waaP*, respectively, suggesting rapid cell lysis. However, cell depletion of the
507 parental strain initiates at 0.063 μg/mL colistin and a complete cell clearance occurs at a
508 concentration higher than 1 μg/mL (Figure 4b). As a result, at a low colistin level (0.195 μg/mL in
509 Figure 5b), the three core mutants are hypersensitive to colistin and are immediately lysed, whereas
510 the parental strain keeps an intact outer membrane to resist NPN, leading to the strongest NPN
511 uptake discrepancy between mutants and the parental strain among the tested colistin levels (Figure
512 5b). At an intermediate colistin level (0.195 to 0.781 μg/mL in Figure 5b), because the rate at which
513 cell lysis occurs for the parental strain increases (Figure 4b) while the mutants remain hypersensitive
514 to colistin, the NPN uptake discrepancy between the mutants and the parental strain decreases with
515 an increasing colistin concentration. When colistin exceeds 1 μg/mL, discrepancies between the NPN
516 uptake for the mutants (Δ*waaC*, Δ*waaF*, and Δ*waaP*) and the parental strain are small (Figure 5b),
517 indicating that both parental and mutant strains are lysed quickly at this colistin level, and
518 consequently exposing comparable amount of phospholipids to NPN. The stronger increase of NPN
519 uptake observed in Δ*waaC* and Δ*waaF* but not Δ*waaP* is consistent with the amount of intact core
520 residues in each mutant (Figure 1a). Figure 5c compares the changes of cell electrokinetic properties
521 and outer membrane permeability induced by LPS structural variations. It suggests that increased
522 outer membrane permeability has opposite effects on cell linear electrokinetic mobility and
523 polarizability. In addition, the trend of 3DiDEP trapping voltage matches the trend of NPN uptake,
524 indicating the potential of using 3DiDEP to distinguish cells based on their outer membrane
525 permeability. Together, *E. coli* outer membrane permeability and small molecule uptake strongly
526 correlate with LPS compositional variations, thereby are distinguishable by cell polarizability and
527 electrokinetic mobility (Figure 5c).

528 **4 Conclusion**

529 Using microfluidic electrokinetic approaches, we've shown that *E. coli* carrying various LPS
530 structures can be quickly distinguished by their linear electrokinetic mobility and cell polarizability.
531 The presence of O-antigen in LPS leads to a decrease in the magnitude of linear electrokinetic
532 mobility and an increased polarizability, which creates a less negatively charged but more polarizable
533 cell surface. Correspondingly, O-antigen expression drives a strong resistance to colistin and low
534 outer membrane permeability, which was observed in this study and elsewhere[62]. In contrast,
535 removing most of the core oligosaccharide by *waaC* deletion does not significantly affect cell
536 electrokinetic mobility, but decreases cell polarizability and leaves cells highly susceptible to colistin.

537 Truncating core oligosaccharides but retaining charged groups (e.g. phosphates) in the core by *waaF*
538 deletion results in a strong negative electrokinetic mobility, a significantly increased polarizability,
539 and an intermediate susceptibility and outer membrane permeability to colistin. A less drastic core
540 alteration mediated by deletion of the heptosyltransferase *waaP* leads to a slightly more negative
541 electrokinetic mobility, a strikingly higher polarizability, and a minor decrease in the bacterial
542 resistance to colistin. Importantly, mutations in the *waa* region have been reported to cause reduced
543 outer membrane protein abundance compared to wild-type cells, which may also drive changes in
544 electrokinetic properties of bacteria. For instance, Δ*waaC* and Δ*waaF* mutations have been reported
545 to cause the loss of flagella[52] and a reduced abundance of outer membrane porins, OmpC and
546 BamA[38], compared to the wild-type condition. In contrast, the Δ*waaP* mutant expresses higher levels
547 of flagella and wild-type levels of OmpC and BamA.[38,52] These unanticipated changes to the cell
548 surface may alter charge density and surface conductance of the soft layers around the cell and thus
549 affect electrokinetic properties. Therefore, further proteomic analysis of membrane protein isolates
550 will be needed to disentangle direct effects of LPS changes and porin abundance on these cell surface
551 charge and dielectric properties.

552 In brief, our study finds relationships between *E. coli* LPS glycoforms, cell electrokinetic and
553 dielectric properties, and outer membrane permeability. By depleting LPS biosynthetic enzymes
554 WaaC, WaaF, and WaaP in *E. coli*, we show that core oligosaccharide changes drive changes in cell
555 surface properties that can be detected in microfluidic electrokinetic devices. These results facilitate
556 the development of high-throughput label-free platforms for screening or isolating bacteria based on
557 their LPS structures using microfluidic electrokinetics. In this study, we used genetically induced
558 LPS mutants as models to demonstrate the feasibility and efficacy of our approach, which paves the
559 way for extended applications to identify and profile clinically relevant strains that differ by a variety
560 of LPS modifications, such as modifications in lipid A and O-antigen,[1,10,11,63,64] or capsule
561 expression.

562 **5 Acknowledgments**

563 We Acknowledge Dr. Chris Hayes at UCSB for supplying the *E. coli* strains studied in this work.

564 **6 Funding**

The work was supported by the Department of Energy's Genome Sciences Program grant SCW1039 and the National Science Foundation award number 1150615. H.K. was partly supported by the Kwanjeong Educational Foundation.

7 Author contributions

QW and CRB conceived the study. QW and HK designed and performed the experiments. TMH provided cell strains and guided the cell cultivation. QW, HK, and TMH interpreted the data. All authors wrote the paper.

8 Conflict of interests

The authors declare that the research was conducted in the absence of any commercial or financial relationships that could be construed as a potential conflict of interest.

575 **9 Figures**

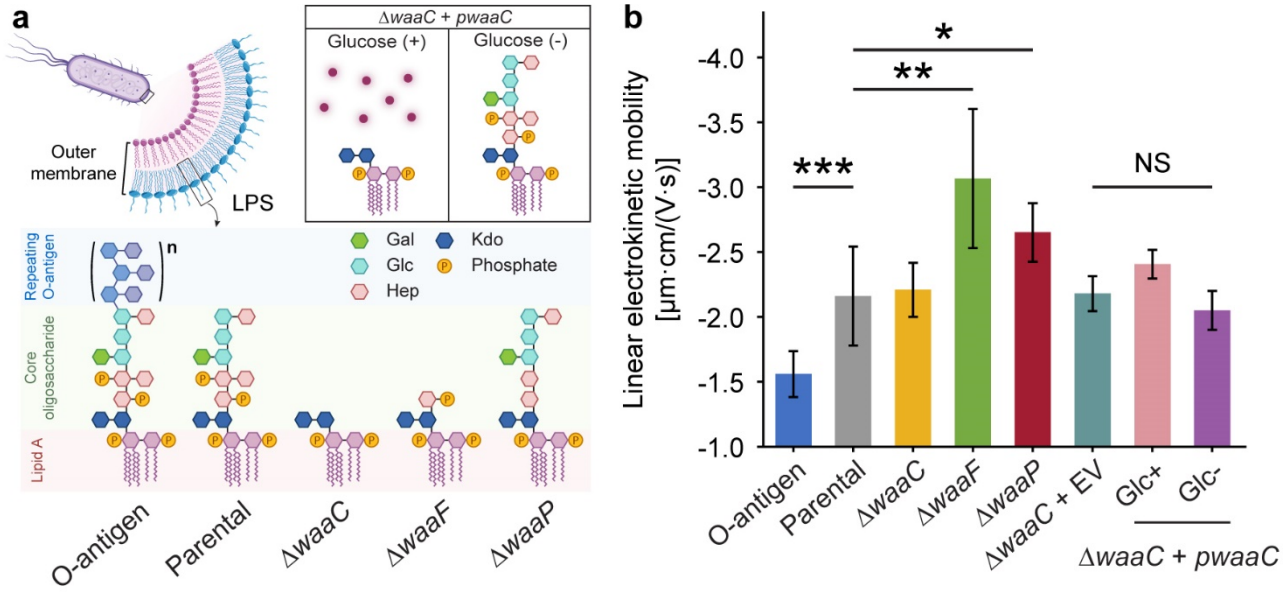

576

577 **Figure 1. Truncating *E. coli* LPS core components affects cell electrokinetic mobility**. (a)
578 Schematic of the expected LPS structures of *E. coli* strains examined in this study. The O-antigen
579 expressing strain is a K-12 strain with restored O16 polysaccharide synthesis. The parental strain
580 expresses full-length LPS without O-antigen. Compared to the parental strain, the Δ*waaC* and Δ*waaF*
581 mutants synthesize shorter LPS without the outer core, leaving only the Kdo_2-lipid A and Hep-Kdo_2-
582 lipid A moieties of the inner core, respectively. The Δ*waaP* strain lacks phosphoryl substituents on
583 HepI and HepII, and is deficient in adding HepIII. The *waaC*-complementary strain (Δ*waaC* +
584 *pwaaC*) carries the plasmid pCH450-*waaC*, whose expression is suppressed in the presence of
585 glucose[38]. Abbreviations: Kdo, 3-Deoxy-D-manno-octulosonic Acid; Hep, L-glycero-D-manno-
586 heptose; Glc, glucose; Gal, galactose. (b) Linear electrokinetic mobilities measured for *E. coli* strains
587 using cell tracking analysis in 60 μm deep straight microchannels and PIV analysis in the main
588 channels of 3DiDEP devices (corresponding to Figure 2a). Results from the two approaches are
589 consistent (Supplementary Figure 1c). Statistical difference for data in this study was analyzed using
590 Kruskal-wallis tests unless otherwise mentioned. Asterisks and error bars in (b) indicate statistical
591 difference (*$p < 0.02$, **$p < 0.005$, and ***$p < 0.001$, NS: not significant) and standard deviations,
592 respectively.

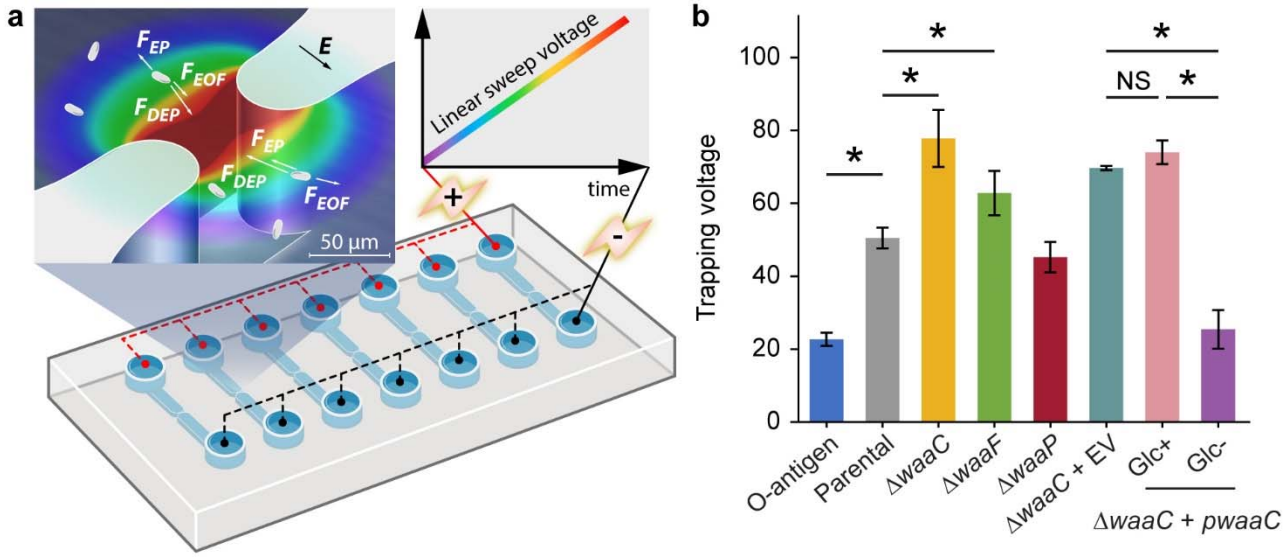

Figure 2. Immobilizing LPS mutants using 3D insulator-based dielectrophoresis (3DiDEP). (a) Schematic of a microfluidic device with an array of 3DiDEP microchannels. A DC potential difference increasing linearly with time at 1 V/s was applied across the channel. Magnified view of the 3D constricted region depicts the 3DiDEP trapping principle: bacteria near the constriction are immobilized when the DEP force balances drag forces due to background electroosmotic (EOF) flow and electrophoresis (EP). Electric field intensity is illustrated in the background color scale (dark red indicates higher values). (b) Measured trapping voltage (threshold voltage at the onset of cell trapping) for each strain. Error bars indicate standard deviations. Asterisks indicate statistical difference (*$p < 0.05$, NS: not significant).

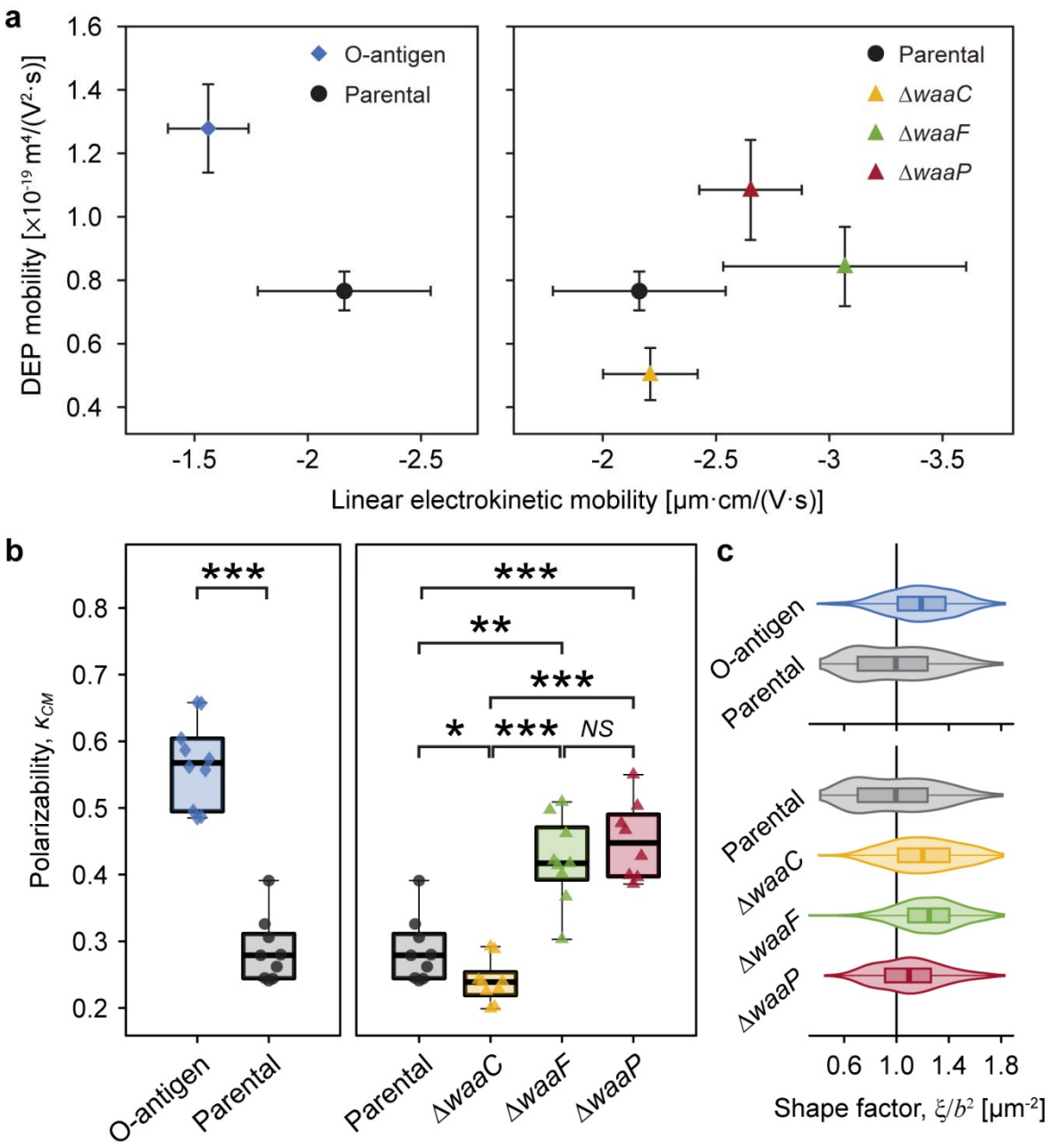

Figure 3. Strong correlation between *E. coli* LPS structural variations, DEP mobilities, and polarizability. (a) Plot of measured DEP mobilities against linear electrokinetic mobilities for each strain indicates that *E. coli* expressing O-antigen (diamond, left) and core synthesis mutants (triangles, right) clearly deviate from the parental strain (circle). Error bars indicate standard deviations. Statistical difference of DEP mobilities is shown in Supplementary Figure 3. (b) Cell polarizability, as measured by Clausius-Mossotti factor (κ_{CM}) of each strain. Asterisks indicate statistical difference (*$p < 0.02$, **$p < 0.005$, and ***$p < 0.001$, NS: not significant). (c) Cell shape factor, ξ/b^2, of studied strains, where ξ is the Perrin friction factor[58] and b is the short semi-axis of

612 the cell. The shape factor represents how much the ellipsoidal cell shape influences the drag force
613 versus the DEP force. See Supplementary Information for a detailed explanation.

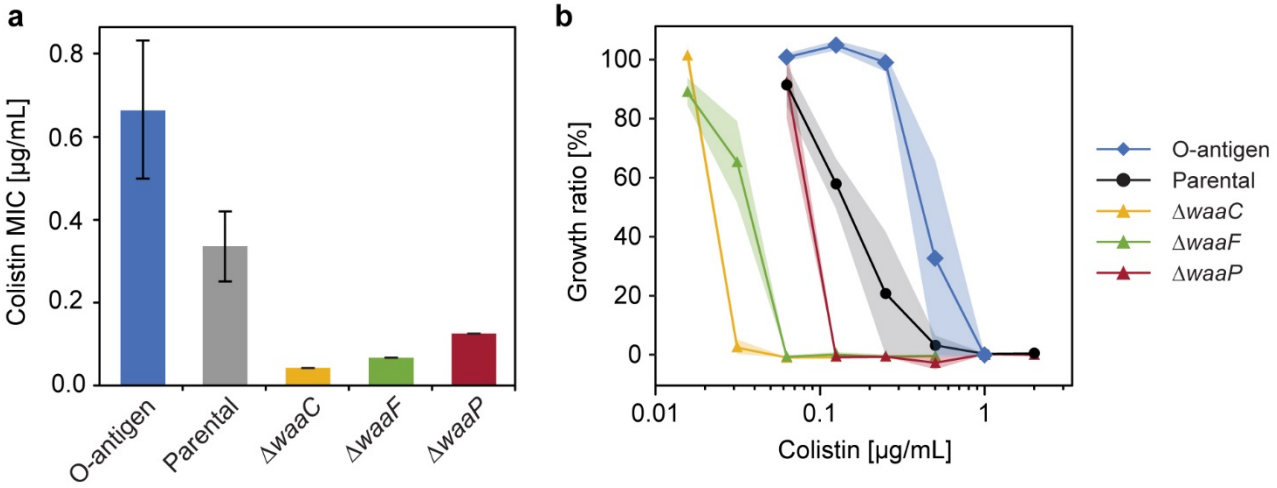

614

615 **Figure 4. Variations in *E. coli* LPS structures affect bacterial response to colistin.** (a) Minimum
616 inhibitory concentration (MIC) of colistin tested for *E. coli* strains expressing different LPS
617 structures ($n = 3$, error bars indicate standard error). (b) Growth inhibition of *E. coli* O-antigen
618 expressing strain (diamonds), parental strain (circles), and mutants with truncated core
619 oligosaccharide (triangles) exposed to varying colistin concentrations. Shaded areas indicate standard
620 errors of three replicates.

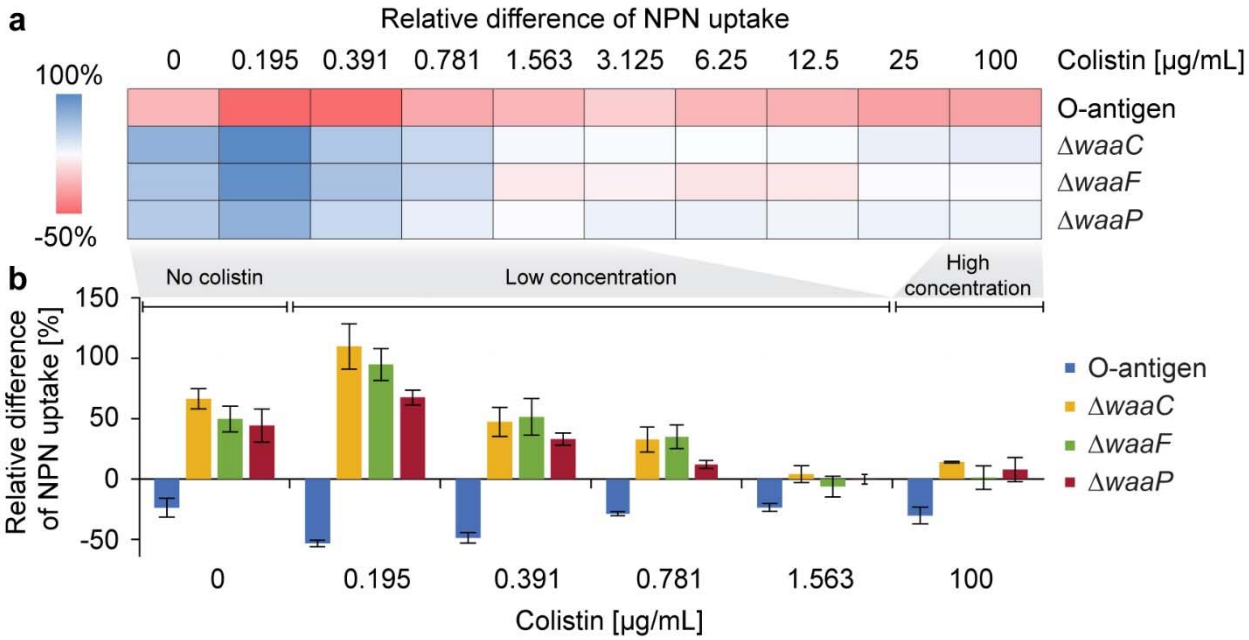

c

Strain		Parental	O-antigen expressing	Δ*waaC*	Δ*waaF*	Δ*waaP*
Presence of LPS components	O-antigen	-	+	-	-	-
	Outer core	+	+	-	-	+
	Inner core	+	+	Only Kdo_2	Kdo_2 and a phosphorylated HepI	Kdo_2, HepI, and HepII
Electrokinetic properties	Electrokinetic mobility	0	-28%	+2%	+49%	+23%
	DEP mobility	0	+67%	-34%	+17%	+42%
	Polarizability	0	+98%	-16%	+47%	+58%
	Trapping voltage	0	-55%	+54%	+24%	-10%
Outer membrane permeability	Colistin MIC	0	+100%	-90%	-81%	-63%
	NPN uptake	0	-53%	+110%	+95%	+68%

Figure 5. Effects of *E. coli* LPS structural variations on colistin-mediated outer-membrane disruption. (a) A heat map showing the mean relative differences of N-Phenyl-1-naphthylamine (NPN) uptake compared to the parental strain for the *E. coli* O-antigen expressing strain and mutants with truncated core oligosaccharide (as computed by Equation 3 in Methods). NPN uptake represents the ratio of background (absence of NPN) subtracted fluorescence values of the bacterial suspension to that of the suspending medium normalized by the cell abundance (details in Methods). (b) Bar plot showing the relative differences of NPN uptake for the O-antigen expressing strain and LPS core mutants at low (0 to 1.563 μg/mL) and high (100 μg/mL) colistin concentrations. The zero line corresponds to the NPN uptake level of the parental strain. Error bars indicate standard errors of three replicates. (c) A table comparing expressed LPS components, electrokinetic properties, and outer

632 membrane permeability of each strain. The ‘+’ / ‘-’ signs indicate the presence/absence of a
633 corresponding LPS component. Percentages indicate the deviation of mean values relative to that of
634 the parental strain.

635 **Reference**

636 1. Raetz, C. R. H. & Whitfield, C. Lipopolysaccharide endotoxins. *Annu. Rev. Biochem.* **71**, 635–
637 700 (2002).

638 2. Klein, G. & Raina, S. Regulated Assembly of LPS, Its Structural Alterations and Cellular
639 Response to LPS Defects. *Int. J. Mol. Sci.* **20**, (2019).

640 3. Simpson, B. W. & Trent, M. S. Pushing the envelope: LPS modifications and their
641 consequences. *Nat. Rev. Microbiol.* **17**, 403–416 (2019).

642 4. Caroff, M. & Novikov, A. LPS Structure, Function, and Heterogeneity. in *Endotoxin Detection*
643 *and Control in Pharma, Limulus, and Mammalian Systems* (ed. Williams, K. L.) 53–93
644 (Springer International Publishing, 2019).

645 5. Needham, B. D. & Trent, M. S. Fortifying the barrier: the impact of lipid A remodelling on
646 bacterial pathogenesis. *Nat. Rev. Microbiol.* **11**, 467–481 (2013).

647 6. Harris, T. L. *et al.* Small molecule downregulation of PmrAB reverses lipid A modification and
648 breaks colistin resistance. *ACS Chem. Biol.* **9**, 122–127 (2014).

649 7. Wang, Z., Wang, J., Ren, G., Li, Y. & Wang, X. Influence of Core Oligosaccharide of
650 Lipopolysaccharide to Outer Membrane Behavior of Escherichia coli. *Mar. Drugs* **13**, 3325–
651 3339 (2015).

652 8. Yethon, J. A., Heinrichs, D. E., Monteiro, M. A., Perry, M. B. & Whitfield, C. Involvement of
653 waaY, waaQ, and waaP in the Modification of Escherichia coliLipopolysaccharide and Their
654 Role in the Formation of a Stable Outer Membrane*. *J. Biol. Chem.* **273**, 26310–26316 (1998).

655 9. Lerouge, I. & Vanderleyden, J. O-antigen structural variation: mechanisms and possible roles in
656 animal/plant-microbe interactions. *FEMS Microbiol. Rev.* **26**, 17–47 (2002).

657 10. Bogomolnaya, L. M., Santiviago, C. A., Yang, H.-J., Baumler, A. J. & Andrews-Polymenis, H.
658 L. 'Form variation' of the O12 antigen is critical for persistence of Salmonella Typhimurium in
659 the murine intestine. *Mol. Microbiol.* **70**, 1105–1119 (2008).

660 11. Kim, M. L. & Slauch, J. M. Effect of acetylation (O-factor 5) on the polyclonal antibody
661 response to Salmonella typhimurium O-antigen. *FEMS Immunol. Med. Microbiol.* **26**, 83–92
662 (1999).

663 12. Gunn, J. S. Bacterial modification of LPS and resistance to antimicrobial peptides. *J. Endotoxin*

664 *Res.* **7**, 57–62 (2001).

665 13. Raetz, C. R. H., Reynolds, C. M., Trent, M. S. & Bishop, R. E. Lipid A modification systems in
666 gram-negative bacteria. *Annu. Rev. Biochem.* **76**, 295–329 (2007).

667 14. Reynolds, C. M., Kalb, S. R., Cotter, R. J. & Raetz, C. R. H. A phosphoethanolamine transferase
668 specific for the outer 3-deoxy-D-manno-octulosonic acid residue of Escherichia coli
669 lipopolysaccharide. Identification of the eptB gene and Ca2+ hypersensitivity of an eptB
670 deletion mutant. *J. Biol. Chem.* **280**, 21202–21211 (2005).

671 15. Tsai, C. M. & Frasch, C. E. A sensitive silver stain for detecting lipopolysaccharides in
672 polyacrylamide gels. *Anal. Biochem.* **119**, 115–119 (1982).

673 16. Kilár, A., Dörnyei, Á. & Kocsis, B. Structural characterization of bacterial lipopolysaccharides
674 with mass spectrometry and on- and off-line separation techniques. *Mass Spectrom. Rev.* **32**, 90–
675 117 (2013).

676 17. Tokel, O. *et al.* Portable microfluidic integrated plasmonic platform for pathogen detection. *Sci.*
677 *Rep.* **5**, 9152 (2015).

678 18. Niu, J. *et al.* Femtomolar Detection of Lipopolysaccharide in Injectables and Serum Samples
679 Using Aptamer-Coupled Reduced Graphene Oxide in a Continuous Injection-Electrostacking
680 Biochip. *Anal. Chem.* **91**, 2360–2367 (2019).

681 19. Yoo, J. H., Woo, D. H., Chang, M.-S. & Chun, M.-S. Microfluidic based biosensing for
682 Escherichia coli detection by embedding antimicrobial peptide-labeled beads. *Sens. Actuators B*
683 *Chem.* **191**, 211–218 (2014).

684 20. Mannoor, M. S., Zhang, S., Link, A. J. & McAlpine, M. C. Electrical detection of pathogenic
685 bacteria via immobilized antimicrobial peptides. *Proc. Natl. Acad. Sci. U. S. A.* **107**, 19207–
686 19212 (2010).

687 21. Kilár, A., Farkas, V., Kovács, K., Kocsis, B. & Kilár, F. Novel quantitative electrophoretic
688 analysis of endotoxins on microchips. *Electrophoresis* **29**, 1713–1722 (2008).

689 22. Makszin, L. *et al.* Quantitative microfluidic analysis ofS- andR-type endotoxin components with
690 chip capillary electrophoresis. *Electrophoresis* **33**, 3351–3360 (2012).

691 23. Wang, X., Zhang, C., Shi, F. & Hu, X. Purification and Characterization of Lipopolysaccharides.
692 in *Endotoxins: Structure, Function and Recognition* (eds. Wang, X. & Quinn, P. J.) 27–51

693 (Springer Netherlands, 2010).

694 24. Hickman, J. & Ashwell, G. Isolation of a bacterial lipopolysaccharide from Xanthomonas
695 campestris containing 3-acetamido-3,6-dideoxy-D-galactose and D-rhamnose. *J. Biol. Chem.*
696 **241**, 1424–1428 (1966).

697 25. Galanos, C., Lüderitz, O. & Westphal, O. A new method for the extraction of R
698 lipopolysaccharides. *Eur. J. Biochem.* **9**, 245–249 (1969).

699 26. Braff, W. A., Pignier, A. & Buie, C. R. High sensitivity three-dimensional insulator-based
700 dielectrophoresis. *Lab Chip* **12**, 1327–1331 (2012).

701 27. Hawkins, B. G., Smith, A. E., Syed, Y. A. & Kirby, B. J. Continuous-flow particle separation by
702 3D Insulative dielectrophoresis using coherently shaped, dc-biased, ac electric fields. *Anal.*
703 *Chem.* **79**, 7291–7300 (2007).

704 28. Lapizco-Encinas, B. H. On the recent developments of insulator-based dielectrophoresis: A
705 review. *Electrophoresis* **40**, 358–375 (2019).

706 29. Jones, P. V. *et al.* Biophysical separation of Staphylococcus epidermidis strains based on
707 antibiotic resistance. *Analyst* **140**, 5152–5161 (2015).

708 30. Braff, W. A., Willner, D., Hugenholtz, P., Rabaey, K. & Buie, C. R. Dielectrophoresis-based
709 discrimination of bacteria at the strain level based on their surface properties. *PLoS One* **8**,
710 e76751 (2013).

711 31. Wang, Q., Jones, A.-A. D., 3rd, Gralnick, J. A., Lin, L. & Buie, C. R. Microfluidic
712 dielectrophoresis illuminates the relationship between microbial cell envelope polarizability and
713 electrochemical activity. *Sci Adv* **5**, eaat5664 (2019).

714 32. Crowther, C. V., Sanderlin, V., Hayes, M. A. & Gile, G. H. Effects of surface treatments on
715 trapping with DC insulator-based dielectrophoresis. *Analyst* **144**, 7478–7488 (2019).

716 33. Wang, Q., Dingari, N. N. & Buie, C. R. Nonlinear electrokinetic effects in insulator-based
717 dielectrophoretic systems. *Electrophoresis* **38**, 2576–2586 (2017).

718 34. Duval, J. F. L. & Ohshima, H. Electrophoresis of diffuse soft particles. *Langmuir* **22**, 3533–3546
719 (2006).

720 35. Ohshima, H. Electrokinetic phenomena of soft particles. *Curr. Opin. Colloid Interface Sci.* **18**,
721 73–82 (2013).

722 36. Francius, G. *et al.* Bacterial surface appendages strongly impact nanomechanical and
723 electrokinetic properties of Escherichia coli cells subjected to osmotic stress. *PLoS One* **6**,
724 e20066 (2011).

725 37. Chandraprabha, M. N., Modak, J. M. & Natarajan, K. A. Soft-particle model analysis of effect of
726 LPS on electrophoretic softness of Acidithiobacillus ferrooxidans grown in presence of different
727 metal ions. *Colloids Surf. B Biointerfaces* **69**, 1–7 (2009).

728 38. Halvorsen, T. M. *et al.* Lipidation of Class IV CdiA Effector Proteins Promotes Target Cell
729 Recognition during Contact-Dependent Growth Inhibition. *MBio* e0253021 (2021).

730 39. Baba, T. *et al.* Construction of Escherichia coli K-12 in-frame, single-gene knockout mutants:
731 the Keio collection. *Mol. Syst. Biol.* **2**, 2006.0008 (2006).

732 40. Allan, D. B., Caswell, T., Keim, N. C., van der Wel, C. M. & Verweij, R. W. *soft-*
733 *matter/trackpy: Trackpy v0.5.0*. (2021). doi:10.5281/zenodo.4682814.

734 41. Crocker, J. C. & Grier, D. G. Methods of Digital Video Microscopy for Colloidal Studies. *J.*
735 *Colloid Interface Sci.* **179**, 298–310 (1996).

736 42. Skinner, S. O., Sepúlveda, L. A., Xu, H. & Golding, I. Measuring mRNA copy number in
737 individual Escherichia coli cells using single-molecule fluorescent in situ hybridization. *Nat.*
738 *Protoc.* **8**, 1100–1113 (2013).

739 43. Vischer, N. O. E. *et al.* Cell age dependent concentration of Escherichia coli divisome proteins
740 analyzed with ImageJ and ObjectJ. *Front. Microbiol.* **6**, 586 (2015).

741 44. MacNair, C. R. *et al.* Overcoming mcr-1 mediated colistin resistance with colistin in
742 combination with other antibiotics. *Nat. Commun.* **9**, 458 (2018).

743 45. Helander, I. M. & Mattila-Sandholm, T. Fluorometric assessment of gram-negative bacterial
744 permeabilization. *J. Appl. Microbiol.* **88**, 213–219 (2000).

745 46. Ashrafizadeh, S. N., Seifollahi, Z., Ganjizade, A. & Sadeghi, A. Electrophoresis of spherical soft
746 particles in electrolyte solutions: A review. *Electrophoresis* **41**, 81–103 (2020).

747 47. Feldman, M. F. *et al.* The Activity of a Putative Polyisoprenol-linked Sugar Translocase (Wzx)
748 Involved in Escherichia coli O Antigen Assembly Is Independent of the Chemical Structure of
749 the O Repeat*. *J. Biol. Chem.* **274**, 35129–35138 (1999).

750 48. Gronow, S., Brabetz, W. & Brade, H. Comparative functional characterization in vitro of

751 heptosyltransferase I (WaaC) and II (WaaF) from Escherichia coli. *Eur. J. Biochem.* **267**, 6602–
752 6611 (2000).

753 49. Kirby, B. J. & Hasselbrink, E. F., Jr. Zeta potential of microfluidic substrates: 2. Data for
754 polymers. *Electrophoresis* **25**, 203–213 (2004).

755 50. Liang, X. *et al.* E. coli Surface Properties Differ between Stream Water and Sediment
756 Environments. *Front. Microbiol.* **7**, 1732 (2016).

757 51. Adams, P. G., Lamoureux, L., Swingle, K. L., Mukundan, H. & Montaño, G. A.
758 Lipopolysaccharide-induced dynamic lipid membrane reorganization: tubules, perforations, and
759 stacks. *Biophys. J.* **106**, 2395–2407 (2014).

760 52. Nakao, R., Ramstedt, M., Wai, S. N. & Uhlin, B. E. Enhanced biofilm formation by Escherichia
761 coli LPS mutants defective in Hep biosynthesis. *PLoS One* **7**, e51241 (2012).

762 53. Kojima, S. & Nikaido, H. High Salt Concentrations Increase Permeability through OmpC
763 Channels of Escherichia coli*. *J. Biol. Chem.* **289**, 26464–26473 (2014).

764 54. Pysher, M. D. & Hayes, M. A. Electrophoretic and dielectrophoretic field gradient technique for
765 separating bioparticles. *Anal. Chem.* **79**, 4552–4557 (2007).

766 55. Moncada-Hernandez, H., Baylon-Cardiel, J. L., Pérez-González, V. H. & Lapizco-Encinas, B.
767 H. Insulator-based dielectrophoresis of microorganisms: theoretical and experimental results.
768 *Electrophoresis* **32**, 2502–2511 (2011).

769 56. Khoshmanesh, K. *et al.* On-chip separation of Lactobacillus bacteria from yeasts using
770 dielectrophoresis. *Microfluid. Nanofluidics* **12**, 597–606 (2012).

771 57. Dingari, N. N. & Buie, C. R. Theoretical investigation of bacteria polarizability under direct
772 current electric fields. *Langmuir* **30**, 4375–4384 (2014).

773 58. Koenig, S. H. Brownian motion of an ellipsoid. A correction to Perrin's results. *Biopolymers* **14**,
774 2421–2423 (1975).

775 59. Sabnis, A. *et al.* Colistin kills bacteria by targeting lipopolysaccharide in the cytoplasmic
776 membrane. *Elife* **10**, (2021).

777 60. Velkov, T., Thompson, P. E., Nation, R. L. & Li, J. Structure--activity relationships of
778 polymyxin antibiotics. *J. Med. Chem.* **53**, 1898–1916 (2010).

779 61. Nikaido Hiroshi. Molecular Basis of Bacterial Outer Membrane Permeability Revisited.

780 *Microbiol. Mol. Biol. Rev.* **67**, 593–656 (2003).

781 62. Moffatt, J. H., Harper, M. & Boyce, J. D. Mechanisms of Polymyxin Resistance. in *Polymyxin*
782 *Antibiotics: From Laboratory Bench to Bedside* (eds. Li, J., Nation, R. L. & Kaye, K. S.) 55–71
783 (Springer International Publishing, 2019).

784 63. Meredith, T. C. *et al.* Modification of Lipopolysaccharide with Colanic Acid (M-antigen)
785 Repeats in Escherichia coli. *J. Biol. Chem.* **282**, 7790–7798 (2007).

786 64. Gulati, S. *et al.* Enhanced factor H binding to sialylated Gonococci is restricted to the sialylated
787 lacto-N-neotetraose lipooligosaccharide species: implications for serum resistance and evidence
788 for a bifunctional lipooligosaccharide sialyltransferase in Gonococci. *Infect. Immun.* **73**, 7390–
789 7397 (2005).